Article

Ordered DNA Wrapping Switches on Luminescence in Single-Walled Nanotube Dispersions

Helen Cathcart, Valeria Nicolosi, J. Marguerite Hughes, Werner J. Blau, John M. Kelly, Susan J. Quinn, and Jonathan N. Coleman

J. Am. Chem. Soc., **2008**, 130 (38), 12734-12744 • DOI: 10.1021/ja803273s • Publication Date (Web): 30 August 2008

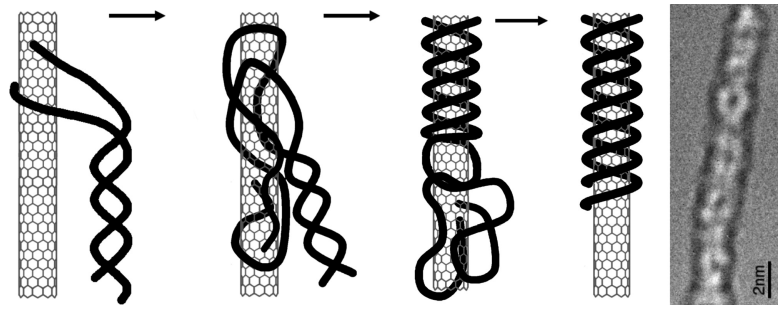

J|A|C|S
ARTICLES

Published on Web 08/30/2008

Ordered DNA Wrapping Switches on Luminescence in Single-Walled Nanotube Dispersions

Helen Cathcart,[†] Valeria Nicolosi,[†] J. Marguerite Hughes,[†] Werner J. Blau,[†] John M. Kelly,[‡] Susan J. Quinn,*[,‡] and Jonathan N. Coleman*[,†,§]

School of Physics, School of Chemistry, and Centre for Research on Adaptive Nanostructures and Nanodevices, Trinity College Dublin, University of Dublin, Dublin 2, Ireland

Received May 8, 2008; E-mail: quinnsu@tcd.ie; colemaj@tcd.ie

Abstract: An extensive study of the time dependence of DNA wrapping in single-walled nanotube (SWNT) dispersions has been carried out, revealing a number of unusual phenomena. SWNTs were dispersed in water with salmon testes DNA and monitored over a three-month period. Between 20 and 50 days after the sample was first prepared, the SWNT photoluminescence (PL) intensity was observed to increase by a factor of 50. This increase was accompanied by a considerable sharpening of the van Hove absorption peaks. High-resolution transmission electron microscopy (HRTEM) images showed the progressive formation of a coating of DNA on the walls of the nanotubes over the three-month period. HRTEM and circular dichroism spectroscopy studies showed that the improvement in both the NIR PL intensity and the van Hove absorption peaks coincided with the completion of a monolayer coating of DNA on the SWNT walls. HRTEM images clearly showed the DNA wrapping helically around the SWNTs in a surprisingly ordered fashion. We suggest that the initial quenching of NIR photoluminescence and broadening of absorption peaks is related to the presence of protonated surface oxides on the nanotubes. The presence of an ordered DNA coating on the nanotube walls mediates both deprotonation and removal of the surface oxides. An extensive DNA coating is required to substantially restore the photoluminescence, and thus, the luminescence switch-on and subsequent saturation indicate the completion of the DNA-wrapping process. The temperature dependence of the PL switch-on, and thus of the wrapping process, was investigated by measuring as functions of temperature both the time before PL switch-on and the time required for the PL intensity to saturate. This allowed the calculation of the activation energies for both the process preceding PL switch-on and the process limiting the rise of PL intensity, which were found to be 31 and 41 kJ mol^{-1}, respectively. The associated entropies of activation were -263 and -225 J mol^{-1} K^{-1}, respectively. These negative activation entropies suggest that the rate-limiting step is characterized by a change in the system from a less-ordered to a more-ordered state, consistent with the formation of an ordered DNA coating.

Introduction

Since their discoveries in 1991[1] and 1993,[2] multiwalled and single-walled carbon nanotubes (SWNTs) have been the subject of intense research because of their excellent mechanical,[3] electrical,[4] and thermal[5] properties. However, difficulties in processing nanotubes, specifically their poor solubility in most common solvents and the tendency of nanotubes to form large bundles, still hamper research efforts. The formation of bundles (which typically contain thousands of SWNTs[6]) makes it impossible to utilize the unique electrical properties of individual nanotubes. Where nanotubes are used for mechanical reinforcement, the presence of bundles reduces the nanotube surface area available for interaction with the surrounding polymer and allows the nanotubes to slide over each other, thereby reducing the effective reinforcement.[7] Where nanotubes are used to prepare conducting polymer composites, the presence of bundles greatly increases the electric percolation threshold.[8] Thus, for many applications, the presence of bundles results in inferior performance.

A variety of different methods, such as liquid-phase dispersion with the aid of polymer wrapping,[9,10] certain solvents,[11−15] surfactants,[16−19] strong acids,[20] surface functionalization,[21,22]

[†] School of Physics.
[‡] School of Chemistry.
[§] Centre for Research on Adaptive Nanostructures and Nanodevices.

(1) Iijima, S. *Nature* **1991**, *354*, 56.
(2) Iijima, S.; Ichihashi, T. *Nature* **1993**, *363*, 603–615.
(3) Coleman, J. N.; Khan, U.; Gun'ko, Y. K. *Adv. Mater.* **2006**, *18*, 689–706.
(4) Wei, B. Q.; Vajtai, R.; Ajayan, P. M. *Appl. Phys. Lett.* **2001**, *79*, 1172–1174.
(5) Berber, S.; Kwon, Y.; Tománek, D. *Phys. Rev. Lett.* **2000**, *84*, 4613–4616.
(6) Zhao, J. Literature Review, University of Cincinnati, 2001.
(7) Cadek, M.; Coleman, J. N.; Ryan, K. P.; Nicolosi, V.; Bister, G.; Fonseca, A.; Nagy, J. B.; Szostak, K.; Beguin, F.; Blau, W. J. *Nano Lett.* **2004**, *4*, 353–356.
(8) Munson-McGee, S. H. *Phys. Rev. B* **1991**, *43*, 3331–3336.
(9) Manchado, M. A. L.; Valentini, L.; Biagiotti, J.; Kenny, J. M. *Carbon* **2005**, *43*, 1499–1505.
(10) Steuerman, D. W. *J. Phys. Chem. B* **2002**, *106*, 3124–3130.
(11) Bergin, S. D.; Nicolosi, V.; Giordani, S.; de Gromard, A.; Carpenter, L.; Blau, W. J.; Coleman, J. N. *Nanotechnology* **2007**, *18*, 455705.
(12) Bergin, S. D.; Nicolosi, V.; Streich, P. V.; Giordani, S.; Sun, Z.; Windle, A. H.; Ryan, P.; Niraj, N. P. P.; Wang, Z.-T. T.; Carpenter, L.; Blau, W. J.; Boland, J. J.; Hamilton, J. P.; Coleman, J. N. *Adv. Mater.* **2008**, *20*, 1–6.

 10.1021/ja803273s CCC: $40.75

and synthetic peptides,[23−26] have been developed for exfoliating nanotubes. One area that shows particular promise is the dispersion of SWNTs in water using DNA.[27−31] SWNTs have been dispersed in water using both natural DNA[27−29] and short, custom-synthesized oligonucleotides.[30,31] These dispersions have the advantage of using water, which is very safe, readily available, and necessary for any potential medical or biological applications, as the solvent. The DNA bonds noncovalently to the nanotube, preserving the nanotubes' electrical and optical properties.[32,33] In addition, DNA-dispersed SWNTs can be separated on the basis of diameter using ion-exchange chromatography[30,31] or by ultracentrifugation through an aqueous density gradient.[34] Additionally, if one chooses, oligonucleotides can be removed using small aromatic molecules such as rhodamine 6G or the cDNA strand once any necessary processing is complete.[32] A variety of different applications, such as fiber spinning,[35] self-assembled nanotube field-effect transistors,[36] stabilization of colloidal particles,[37] chemical sensing,[38] and applications in both medical diagnostic and biological fields[33,39−42] have been investigated for DNA-dispersed SWNTs. However, before DNA−SWNT dispersions can be fully utilized, a greater understanding of the interactions between DNA and nanotubes and the resultant effects on the nanotubes' properties is needed.

It is currently accepted that the DNA wraps helically around the SWNTs, allowing the nucleotide bases to interact with the nanotube walls via π stacking while the backbone creates an interface between the water and the nanotube.[28,30,43] The modes of interaction between the DNA and the nanotube surface for various systems have been simulated by molecular modeling experiments.[44] Studies on short oligonucleotides under conditions of low ionic strength revealed the importance of hydrogen-bonding interactions in the helical wrapping geometry of the single-stranded DNA (ss-DNA).[45] Additional studies also considered the wrapping interactions of long homopolymers[46] and the binding of double-stranded DNA (ds-DNA), including groove-binding interactions.[47,48] A particularly interesting molecular dynamics study by Johnson et al.[49] demonstrated the conformational changes associated with wrapping.

It is generally accepted that the resultant DNA sheath protects the nanotube surface from interacting with the water. Such coatings can be surprisingly ordered; atomic force microscopy (AFM) phase images showing periodic helical wrapping of nanotubes by ss-DNA have been published.[28,31] However, these results do not seem to have been followed up by an in-depth experimental study into the process of formation of DNA coatings.

To date, the majority of studies on DNA−SWNT systems have investigated stabilization by short, synthetic oligonucleotides of known sequence, with some sequence-dependent stabilization considered.[28,30] In contrast to many of these earlier studies, this report considers the evolution of binding of natural DNA present initially in the double-stranded form and comprising a large number of alternating bases (~10 000 base pairs with 41% GC content) in a random sequence. It is reasonable to assume that the time taken for DNA wrapping to occur should be related to the length of the DNA sequence.[50] Intuitively, this is not expected to occur immediately, especially when long, natural ds-DNA is used as the dispersant.[27] A more likely

(13) Furtado, C. A.; Kim, U. J.; Gutierrez, H. R.; Pan, L.; Dickey, E. C.; Eklund, P. C. *J. Am. Chem. Soc.* **2004**, *126*, 6095–6105.
(14) Giordani, S.; Bergin, S. D.; Nicolosi, V.; Lebedkin, S.; Kappes, M. M.; Blau, W. J.; Coleman, J. N. *J. Phys. Chem. B* **2006**, *110*, 15708–15718.
(15) Landi, B. J.; Ruf, H. J.; Worman, J. J.; Raffaelle, R. P. *J. Phys. Chem. B* **2004**, *108*, 17089–17095.
(16) Bergin, S. D.; Nicolosi, V.; Cathcart, H.; Lotya, M.; Rickard, D.; Sun, Z.; Blau, W. J.; Coleman, J. N. *J. Phys. Chem. C* **2008**, *112*, 972–977.
(17) Bachilo, S. M.; Strano, M. S.; Kittrell, C.; Hauge, R. H.; Smalley, R. E.; Weisman, R. B. *Science* **2002**, *298*, 2361–2366.
(18) O'Connell, M. J.; Bachilo, S. H.; Huffman, C. B.; Moore, V. C.; Strano, M. S.; Haroz, E. H.; Rialon, K. L.; Boul, P. J.; Noon, W. H.; Kittrell, C.; Ma, J.; Hauge, R. H.; Weisman, R. B.; Smalley, R. E. *Science* **2002**, *297*, 593–596.
(19) Moore, V. C.; Strano, M. S.; Haroz, E. H.; Hauge, R. H.; Smalley, R. E.; Schmidt, J.; Talmon, Y. *Nano Lett.* **2003**, *3*, 1379–1382.
(20) Penicaud, A.; Poulin, P.; Derre, A. *J. Am. Chem. Soc.* **2005**, *127*, 8–9.
(21) Amiran, J.; Nicolosi, V.; Bergin, S. D.; Khan, U.; Lyons, P. E.; Coleman, J. N. *J. Phys. Chem. C* **2008**, *112*, 3519–3524.
(22) Koshio, A.; Yudasaka, M. *Nano Lett.* **2001**, *1*, 361–363.
(23) Nicolosi, V.; Cathcart, H.; Dalton, A. R.; Aherne, D.; Dieckmann, G. R.; Coleman, J. N. *Biomacromolecules* **2008**, *9*, 598–602.
(24) Ortiz-Acevedo, A.; Xie, H.; Zorbas, V.; Sampson, W. M.; Dalton, A. B.; Baughman, R. H.; Draper, R. K.; Musselman, I. H.; Dieckmann, G. R. *J. Am. Chem. Soc.* **2005**, *127*, 9512–9517.
(25) Dalton, A. B.; Ortiz-Acevedo, A.; Zorbas, V.; Brunner, E.; Sampson, W. M.; Collins, S.; Razal, J. M.; Yoshida, M. M.; Baughman, R. H.; Draper, R. K.; Musselman, I. H.; Jose-Yacaman, M.; Dieckmann, G. R. *Adv. Funct. Mater.* **2004**, *14*, 1147–1151.
(26) Dieckmann, G. R.; Dalton, A. B.; Johnson, P. A.; Razal, J.; Chen, J.; Giordano, G. M.; Munoz, E.; Musselman, I. H.; Baughman, R. H.; Draper, R. K. *J. Am. Chem. Soc.* **2003**, *125*, 1770–1777.
(27) Cathcart, H.; Quinn, S.; Nicolosi, V.; Kelly, J. M.; Blau, W. J.; Coleman, J. N. *J. Phys. Chem. C* **2007**, *111*, 66–74.
(28) Gigliotti, B.; Sakizzie, B.; Bethune, D. S.; Shelby, R. M.; Cha, J. N. *Nano Lett.* **2006**, *6*, 159–164.
(29) Nakashima, N.; Okuzono, S.; Murakami, H.; Nakai, T.; Yoshikawa, K. *Chem. Lett.* **2003**, *32*, 456–457.
(30) Zheng, M.; Jagota, A.; Semke, E. D.; Diner, B. A.; McLean, R. S.; Lustig, S. R.; Richardson, R. E.; Tassi, N. G. *Nat. Mater.* **2003**, *2*, 338–342.
(31) Zheng, M.; Jagota, A.; Strano, M. S.; Santos, A. P.; Barone, P.; Chou, S. G.; Diner, B. A.; Dresselhaus, M. S.; McLean, R. S.; Onoa, G. B.; Samsonidze, G. G.; Semke, E. D.; Usrey, M.; Walls, D. J. *Science* **2003**, *302*, 1545–1548.
(32) Chen, R. J.; Zhang, Y. *J. Phys. Chem. B* **2006**, *110*, 54–57.
(33) Heller, D. A.; Baik, S.; Eurell, T. E.; Strano, M. S. *Adv. Mater.* **2005**, *17*, 2793–2799.
(34) Arnold, M. S.; Stupp, S. I.; Hersam, M. C. *Nano Lett.* **2005**, *5*, 713–718.
(35) Barisci, J. N.; Tahhan, M.; Wallace, G. G.; Badaire, S.; Vaugien, T.; Maugey, M.; Poulin, P. *Adv. Funct. Mater.* **2004**, *14*, 133–138.
(36) Keren, K.; Berman, R. S.; Buchstab, E.; Sivan, U.; Braun, E. *Science* **2003**, *302*, 1380–1382.
(37) Hobbie, E. K.; Bauer, B. J.; Stephens, J.; Becker, M. L.; McGuiggan, P.; Hudson, S. D.; Wang, H. *Langmuir* **2005**, *21*, 10284–10287.
(38) Staii, C.; Johnson, A. T.; Chen, M.; Gelperin, A. *Nano Lett.* **2005**, *5*, 1774–1778.
(39) Heller, D. A.; Jeng, E. S.; Tsun-Kwan, Y.; Martinez, B. M.; Moll, A. E.; Gastala, J. B.; Strano, M. S. *Science* **2006**, *311*, 508–511.
(40) Hu, C.; Zhang, Y.; Bao, G.; Zhang, Y.; Liu, M.; Wang, Z. L. *J. Phys. Chem. B* **2005**, *109*, 20072–20076.
(41) Karachevtsev, V. A.; Glamazda, A. Y.; Leontiev, V. S.; Lytvyn, O. S.; Dettlaff-Weglikowska, U. *Chem. Phys. Lett.* **2007**, *435*, 104–108.
(42) Rao, K. S.; Daniel, S.; Rao, T. P.; Rani, S. U.; Naidu, G. R. K.; Hea-Yeon, L.; Kawai, T. *Sens. Actuators, B* **2007**, *122*, 672–682.
(43) Lustig, S. R.; Jagota, A.; Khripin, C.; Zheng, M. *J. Phys. Chem. B* **2005**, *109*, 2559–2566.
(44) Gao, H. J.; Kong, Y. *Annu. Rev. Mater. Res.* **2004**, *34*, 123–150.
(45) Manohar, S.; Tang, T.; Jagota, A. *J. Phys. Chem. C* **2007**, *111*, 17835–17845.
(46) Karachevtsev, M. V.; Lytvyn, O. S.; Stepanian, S. G.; Leontiev, V. S.; Adamowicz, L.; Karachevtsev, V. A. *J. Nanosci. Nanotechnol.* **2008**, *8*, 1473–1480.
(47) Zhao, X.; Johnson, J. K. *J. Am. Chem. Soc.* **2007**, *129*, 10438–10445.
(48) Lu, G.; Maragakis, P.; Kaxiras, E. *Nano Let.* **2005**, *5*, 897–900.
(49) Johnson, R. R.; Johnson, A. T. C.; Klein, M. L. *Nano Lett.* **2008**, *8*, 69–75.
(50) Vogel, S. R.; Muller, K.; Plutowski, U.; Kappes, M. M.; Richert, C. *Phys. Status Solidi B* **2007**, *244*, 4026–4029.

process would be one in which the conformation of the DNA that coats the nanotube evolves over time.

This transformation from uncoated to fully coated nanotubes is likely to have a marked effect on the optical properties of the SWNT. The optical transition energies of SWNTs are influenced by the dielectric properties of their local surroundings,[51,52] and thus, changes in the degree of DNA wrapping and the level of interaction between the nanotube and the surrounding water are expected, at the very least, to cause changes in the absorption and photoluminescence (PL) peak positions. These changes could mistakenly be attributed to bundling in the sample, which is known to shift peaks, quench luminescence, and broaden absorption peaks.[15,17,18,53−56] The motivation for this work was therefore to obtain a greater understanding of the interactions between DNA and nanotubes and to determine their effect on the optical properties of the system over time.

Results

Absorption and Photoluminescence Spectroscopy. DNA−SWNT samples were prepared using double-stranded B-form salmon testes DNA (41% GC content). The DNA length was found to be ∼10,000 base pairs, but this was expected to decrease somewhat after sample preparation as a result of sonication. The average SWNT length was ∼260 nm after sample preparation.[27] The samples were stored in the dark at room temperature and monitored over a period of 3 months. The UV−vis−NIR absorption spectra are presented in Figure 1A, with some of the spectra omitted for clarity. Significant changes in the absorption spectra, characterized by the transformation from poorly defined absorption peaks to a set of sharp, well-resolved peaks, were observed after ∼35 days. The inset shows an expanded view of two S_{22} peaks in the 600−800 nm wavelength region. These peaks were observed to blue-shift slightly between days 28 and 35. This blue shift is consistent with changes in the nanotubes' local dielectric constant due to shielding from the surrounding water by the DNA.[52] The wavelength of the higher-energy peak was found to shift by 4 nm (from 659 to 655 nm) while the lower-energy peak shifted by 6 nm (from 741 to 735 nm). The peak heights are shown as a function of time in Figure 1B. It was found that both of the S_{22} peak heights increased slightly between days 28 and 35. There were no significant changes in the peak widths (fwhm) over this time period.

The most remarkable changes to the spectrum occurred in the 850−1350 nm region, where S_{11} transitions occur. Initially, the spectrum had no well-defined features in this region. By day 28, a set of very weak peaks could be distinguished from the background absorption. Close to day 35, a major change occurred in the sample, giving rise to the appearance of intense, well-resolved peaks. No significant change in the spectrum was observed after this time. The peak heights are shown as a function of time in Figure 1B. It is clear that all of the peak heights increased between days 28 and 35; however, the increase in peak heights was far more dramatic for the S_{11} transitions (closed symbols) than for the S_{22} transitions (open symbols).

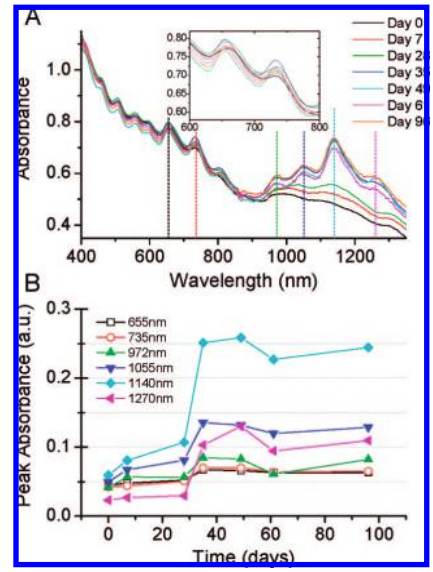

Figure 1. (A) Absorption spectra recorded at various times, showing an increase in the van Hove peak height over time. (B) Peak heights for six van Hove peaks (indicated by the colored, dashed vertical lines) plotted as a function of time. All of the peak heights increased between days 28 and 35, with the most dramatic increases being observed in the S_{11} region.

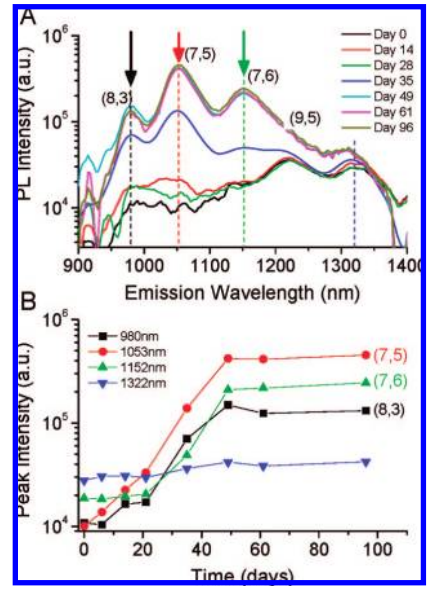

Figure 2. (A) PL spectra excited at 655 nm and recorded at various times, showing the growth of the peak heights over time. (B) Peak heights shown as a function of time.

Similar time-dependent changes in the solution's PL spectra were observed (Figure 2A). The samples were excited at a wavelength of 655 nm. Individual semiconducting nanotubes with chiralities of (8,3), (7,5), (7,6), and (9,5) are expected to emit in this wavelength range.[18] During the first 28 days, there was virtually no detectable PL emission. Two broad, weak peaks were observed at wavelengths of 1220 and 1322 nm. The peak at 1220 nm may be attributed to blue-shifted emission from (9,5) nanotubes, but there are no known emission peaks near 1322 nm. This peak did not shift when the excitation wavelength was varied and is not a harmonic of the excitation wavelength.

(51) Hertel, T.; Hagen, A.; Talalaev, V.; Arnold, K.; Hennrich, F.; Kappes, M.; Rosenthal, S.; McBride, J.; Ulbricht, H.; Flahaut, E. *Nano Lett.* **2005**, *5*, 511–514.
(52) Choi, J. H.; Strano, M. S. *Appl. Phys. Lett.* **2007**, *90*, 223114.
(53) Ryabenko, A. G.; Dorofeeva, T. V.; Zvereva, G. I. *Carbon* **2004**, *42*, 1523–1535.
(54) Tan, Y.; Resasco, D. E. *J. Phys. Chem. B* **2005**, *109*, 14454–14460.
(55) Weisman, R. B.; Bachilo, S. M.; Tsyboulski, D. *Appl. Phys. A: Mater. Sci. Process.* **2004**, *78*, 1111–1116.
(56) Hartschuh, A.; Pedrosa, H. N.; Novotny, L.; Krauss, T. D. *Science* **2003**, *301*, 1354–1356.

The peaks are thought to originate from small bundles containing only semiconducting nanotubes, where interactions between adjacent nanotubes cause the emission to become significantly broadened and red-shifted. The heights of these peaks did not change significantly over the duration of the experiment. Between days 28 and 35, a major change occurred in the sample that caused the PL to "switch on", giving rise to a set of strong PL emission peaks. The intensities of these peaks grew further throughout the following week, yielding an intense, well-defined PL spectrum by day 49. No significant changes in the peak intensities were observed after this time. The peak heights are plotted as a function of time in Figure 2B, which again shows that the greatest intensity changes occurred between days 28 and 49. PL maps of the sample showed similar time-dependent changes in the emission intensities of a variety of other semiconducting nanotubes (Figure S1 in the Supporting Information). Interestingly, the set of emission peaks corresponding to large-diameter nanotubes that are usually observed at longer emission wavelengths were not detected, even after 100 days. As the quantum efficiency of nanotubes decreases with increasing nanotube diameter,[57] it was expected that the emission from the larger-diameter nanotubes would be less intense than for the smaller-diameter nanotubes. However, in these samples the large-diameter peaks were missing altogether. There are two possible reasons for this: either the DNA is selectively debundling the smaller-diameter nanotubes while the larger-diameter nanotubes remain in bundles, or else the interactions between DNA and the nanotubed differ on the basis of diameter, resulting in strong PL quenching for large-diameter nanotubes even after 100 days. The first possibility seems unlikely, as adsorption of polymers at the surface of nanotubes is known to be less favorable for smaller-diameter nanotubes. The nanotube curvature influences the number of polymer configurations possible in the bound state. In the case of larger-diameter nanotubes, the polymer may adsorb with a larger number of possible conformations, making adsorption more likely.[58]

pH Effects Due to Sonication. It is known that sonication of aqueous samples can lead to a reduction in pH[59] and that the protons so produced can cause quenching of the photoluminescence of SWNTs.[60,61] This quenching effect is generally observed for pH < 6.[59,61] Thus, it was possible that the observed spectroscopic changes could be attributed to a sonication-induced decrease in pH followed by a slow increase in pH over time. To test this, we checked the pH of a number of samples immediately after sonication. It was found that in all of the samples measured, the pH shortly after sonication was always above 6.5. In addition, the pH was measured again 2 months later (after the PL had saturated) and was found to be unchanged within error. Therefore, the changes in the PL and absorption intensities cannot be attributed to a slow, time-dependent change in the pH of the sample.

Atomic Force Microscopy Measurement of Bundle Size. In order to rule out the possibility that changes in the number of individually dispersed SWNTs caused the changes in the nanotube optical properties, AFM images of deposited samples were recorded weekly to monitor the bundle diameter distribution (Figure S2 in the Supporting Information). It was found that a large population of very small bundles/nanotubes with diameters of <2 nm was present at all times throughout the experiment. The mean diameter is plotted as a function of time in the top panel of Figure 3. It can be seen that during the first 2 weeks, the mean diameter increased slightly, to 2.4 nm from an initial value of 1.5 nm, before decreasing again and settling at a mean value of 2 nm after day 28.

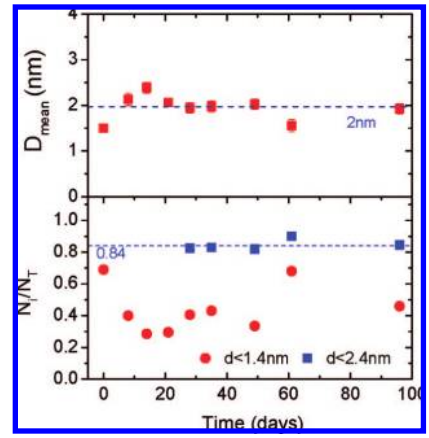

Figure 3. (top) Mean bundle diameter and (bottom) number fraction of individual SWNTs calculated from AFM images, shown as functions of time. The mean diameter was found to settle at a mean diameter of 2 nm after day 35. The fraction of individual SWNTs was calculated using a cutoff value of 1.4 nm (SWNTs only) or 2.4 nm (DNA−SWNT hybrid).

We propose that the changes in the diameter distribution represent the progression from unwrapped to wrapped SWNTs. Initially, the diameters are very small because the DNA is only loosely associated with the nanotubes, leaving large areas of the nanotube walls uncovered. Thus, to a first approximation, the diameter distributions at this time represent the diameters of the nanotubes alone.[62] However, over time the DNA rearranges itself on the walls of the nanotube and finds its optimum conformation, tightly wrapped around the nanotube (see below).[28,58] The added contribution of the DNA to the hybrid diameter results in the apparent increase in diameter as measured by AFM at longer times. The diameters observed at these times are similar to values quoted elsewhere for DNA-wrapped nanotubes.[30] Between these two stages, there must exist a period where the DNA is interacting with the nanotube but is not tightly wrapped around it. During this period, the contribution of the DNA to the hybrid diameter may vary significantly, depending on the degree of coverage, the way in which the DNA interacts with the nanotube, and whether the DNA is completely denatured into two single strands or still partially double-stranded.

The fraction of individually dispersed SWNTs (N_i/N_T), which was calculated from the diameter distributions using a cutoff value of 1.4 nm, is presented in the bottom panel of Figure 3.[14] Initially, this value was very high, indicating that despite the lack of photoluminescence, a large population of individual SWNTs was present at this time. However, because the cutoff diameter did not allow for the contribution of the DNA to the

(57) Reich, S.; Thomsen, C.; Robertson, J. *Phys. Rev. Lett.* **2005**, *95*, 077402.
(58) Gurevitch, I.; Srebnik, S. *Chem. Phys. Lett.* **2007**, *444*, 96–100.
(59) Benedict, B.; Pehrsson, P. E.; Zhao, W. *J. Phys. Chem. B* **2005**, *109*, 7778–7780.
(60) Zhao, W.; Song, C.; Pehrsson, P. E. *J. Am. Chem. Soc.* **2002**, *124*, 12418–12419.
(61) Strano, M. S.; Huffman, C. B.; Moore, V. C.; O'Connell, M. J.; Haroz, E. H.; Hubbard, J.; Miller, M.; Rialon, K.; Kittrell, C.; Ramesh, S.; Hauge, R. H.; Smalley, R. E. *J. Phys. Chem. B* **2003**, *107*, 6979–6985.
(62) Malik, S.; Vogel, S.; Rosner, H.; Arnold, K.; Hennrich, F.; Kohler, A.-K.; Richert, C.; Kappes, M. M. *Compos. Sci. Technol.* **2007**, *67*, 916–921.

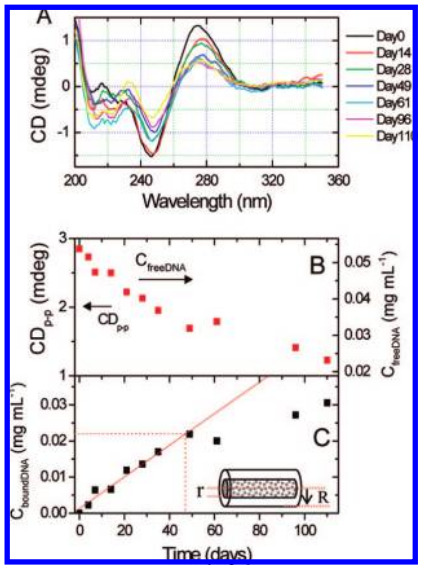

Figure 4. (A) CD spectra recorded at different times over a three-month period. The magnitude of the spectra was found to decrease continuously over the duration of the experiment. (B) CD peak-to-peak height (left axis) and calculated concentration of free DNA (right axis) as a function of time. (C) Concentration of bound DNA as a function of time. The dotted line shows the time at which a full monolayer coats the SWNTs. The concentration of bound DNA was found to increase linearly up to this time and sublinearly thereafter.

hybrid diameter, the number fraction appeared to decrease over the following weeks as DNA wrapping took place. For comparison, the values of N_i/N_T for the later stages of the experiment were recalculated to include an approximate DNA contribution of 1 nm to the hybrid diameter (i.e., a cutoff value of 2.4 nm was used). It was found that when DNA coverage was included, the number fraction after day 30 stayed relatively constant at a value of 0.84 ± 0.04 (Figure 3, bottom panel). This is an important observation, as it leads to the conclusion that the fraction of individual nanotubes remains constant with time. While this is certainly true after day 30, we believe the population of individual nanotubes is constant during the whole experiment (90 days). Thus, the AFM data shows that it is unlikely that the changes in the nanotubes' optical properties can be correlated to a change in the population of individual SWNTs. However, it must be noted that the improvement in the absorption and PL spectra coincides with the time at which the fluctuations in the mean diameters stabilize. If our understanding of these variations is correct, then the reorganization of DNA on the nanotube surface to yield a more complete surface coverage via tighter wrapping could be responsible for the changes in the optical properties of the system.

Circular Dichroism Spectroscopy. Circular dichroism (CD) is very sensitive to the helical structure of ds-DNA in solution.[63,64] CD measurements were carried out weekly on the solution in order to check for changes in the DNA conformation. The obtained CD spectra were typical of B-form ds-DNA[65] (Figure 4A). The magnitude of the spectrum was found to decrease continuously throughout the experiment, while the spectral shape did not change significantly over time. The plot of CD peak-to-peak height as a function of time (Figure 4B) clearly shows the continual decrease in CD intensity.

We suggest that these spectra can be interpreted by considering the fraction of free DNA in solution. The free DNA is not bound to any nanotubes and is free to adopt the usual B form in water. Initially ($t = 0$), the majority of the DNA is free in solution in the double-stranded form, so the CD intensity is at its maximum. We propose that the overall CD intensity decreases as as an increasing amount of DNA adsorbs onto the nanotube walls and that this reduction results from the disruption of stacking between adjacent nucleotide bases that is associated with the DNA going from free double-stranded to adsorbed single-stranded form. When a strand of DNA wraps around a nanotube, the nucleotide bases rotate and interact with the walls of the nanotube via base−nanotube stacking interactions.[30,43] Thus, the conformation of the backbone changes, and the stacking between bases is disrupted. This can lead to a large decrease in the CD intensity.[63] For example, the CD intensity of adenylyl-3′-5′-adenosine (ApA) is a factor of 10 times greater than that of adenosine alone as a result of interactions between the stacked bases.[64] Thus, when wrapping occurs, the contribution from base−base stacking interactions disappears, and the CD intensity decreases dramatically. In addition, it is possible that electronic coupling between the nucleotide bases and the SWNTs[66,67] leads to a decrease in the DNA absorbance intensity, thereby further decreasing the CD intensity. This would account for the slight decrease in the DNA absorption seen at later times (Figure S3 in the Supporting Information) Thus, as the DNA wraps around the nanotube, the CD effectively switches off. Such a phenomenon is routinely observed when ds-DNA is transformed to ss-DNA in the presence of a denaturant.[68] Consequently, the time-dependent reduction in the CD intensity can be interpreted as a shift from a phase dominated by free ds-DNA to one dominated by bound ss-DNA, as the DNA coats the nanotube over time. Thus, the reduction of the CD signal offers an effective indirect method of observing DNA adsorption on the surface. It should be noted that this is a reasonably straightforward method compared with techniques such as fluorescence labeling, which requires synthesis of labeled nucleotides.

It is possible to calculate the relationship between the CD peak-to-peak height and the concentration of free ds-DNA in solution (Figure S3 in the Supporting Information). To do this, CD spectra were recorded for a number of DNA-only solutions (assumed to contain only ds-DNA) with concentrations ranging from 0.05 to 0.009 mg mL^{-1}. This was used to transform the CD peak-to-peak heights for the nanotube dispersions into the concentration of free DNA ($C_{freeDNA}$). It was found that $C_{freeDNA}$ on day 0 was ~0.053 mg mL^{-1}, matching the concentration of DNA in the solution as first prepared (0.05 mg mL^{-1}) within the error of the spectropolarimeter. This suggests that while nanotube bundles sediment out of solution during centrifugation, all of the DNA remains, effectively increasing the ratio of DNA to SWNTs after centrifugation to a value of 2.8:1.

The concentrations of free and bound DNA ($C_{boundDNA} = C_{totalDNA} - C_{freeDNA}$) are plotted as functions of time in panels B and C, respectively, of Figure 4. This data clearly shows that $C_{boundDNA}$ increased linearly with time up to $t \approx 45$ days, after

(63) Cantor, C. R.; Warshaw, M. M.; Shapiro, H. *Biopolymers* **1970**, *9*, 1059–1077.
(64) Warshaw, M. M.; Cantor, C. R. *Biopolymers* **1970**, *9*, 1079–1103.
(65) Bloomfield, V. A.; Crothers, D. M.; Tinoco, I. *Nucleic Acids: Structures, Properties and Functions*; University Science Books: Mill Valley, CA, 2000.
(66) Meng, S.; Maragakis, P.; Papaloukas, C.; Kaxiras, E. *Nano Lett.* **2007**, *7*, 45–50.
(67) Snyder, S. E.; Rotkin, S. V. *JETP Lett.* **2006**, *84*, 348–351.
(68) Balkwill, G. D.; Williams, H. E. L.; Searle, M. S. *Org. Biomol. Chem.* **2007**, *5*, 832–839.

which the rate of increase declined. It is possible to calculate to a first approximation the time at which a full monolayer of DNA covers the nanotubes using the following model. First, we make the approximation that the bound DNA fully coats the nanotube with a uniform coating (as shown schematically in the inset of Figure 4C), yielding a hybrid radius R for a given nanotube of radius r and length L. Thus, we can write that

$$\frac{C_{\text{boundDNA}}}{C_{\text{NT}}} = \frac{\rho_{\text{DNA}}(R^2 - r^2)\pi L}{\rho_{\text{NT}} r^2 \pi L} \quad (1)$$

giving

$$C_{\text{boundDNA}} = C_{\text{NT}} \frac{\rho_{\text{DNA}}}{\rho_{\text{NT}}}\left[\left(\frac{R}{r}\right)^2 - 1\right] \quad (2)$$

where C_{NT} is the concentration of the nanotubes and ρ_{DNA} and ρ_{NT} are the densities of DNA and nanotubes, respectively.

To a first approximation, one can assume that for a nanotube coated with a monolayer of DNA, $r \approx 0.5$ nm, $R \approx 1$ nm, $\rho_{\text{NT}} \approx 1500$ kg m^{-3},[69] and $\rho_{\text{DNA}} \approx 625$ kg m^{-3} (see Figure S4 and the accompanying text in the Supporting Information); substitution of these values into eq 2 indicates that when a full monolayer coats the nanotube, the concentration of bound DNA is $C_{\text{boundDNA}} = 0.022$ mg mL^{-1} when $C_{\text{NT}} = 0.018$ mg mL^{-1}. Referring to Figure 4C, we find that this concentration of bound DNA occurred on approximately day 47, indicating that a full monolayer of DNA coated the nanotubes at this time. This is a very exciting result, because this time at which a full DNA monolayer coated the nanotubes coincided with the time at which the PL spectra were fully switched on (Figure 2). It should also be noted that the concentration of bound DNA increased linearly up to this point but increased sublinearly after this time. This is not surprising, as the binding affinity between DNA and nanotubes is expected to be different than that of DNA to itself; thus, once a full layer of DNA coats the nanotube, one would expect the binding rate to change.

High-Resolution Transmission Electron Microscopy. In order to verify this interpretation of the CD results, high-resolution transmission electron microscopy (HRTEM) images of the sample were recorded regularly, allowing one to observe the DNA−SWNT complex in detail. Representative images of the DNA−SWNT complexes recorded at different times throughout the three-month duration of the experiment are shown in Figure 5. These images clearly show that the DNA progressively coated the nanotube over time. On day 1, the DNA appeared to be clustered haphazardly around the nanotube bundles, and large areas of the nanotubes were uncoated by DNA. The nanotube walls could be clearly distinguished from their surroundings at this time. These images are similar to HRTEM images of SWNTs dispersed with oligonucleotides presented elsewhere.[62] By day 16, the DNA coverage had increased, but significant areas of the nanotube walls still remained uncoated. The diameter of the hybrid varied significantly along its length at this time. By day 21, DNA could be seen to cover most of the nanotube, and on day 35, almost all of the nanotube walls were coated with a thin layer of DNA. In fact, analysis of a number of images suggested that on average, one monolayer of DNA coated each nanotube by day 35. This agrees reasonably well with the CD-derived estimate of 47 days for the formation of a monolayer. Finally, by day 96, a thick layer of DNA covered the nanotubes, making it impossible to distinguish the nanotube walls from the surrounding DNA.

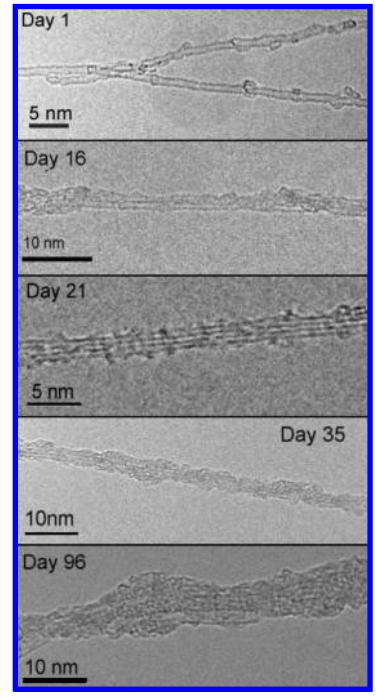

Figure 5. Representative HRTEM images showing both single nanotubes and small bundles at various times. The time-dependent formation of the DNA coating on the nanotubes can be seen clearly.

These results are extremely exciting and show overwhelming evidence for the progressive formation of a DNA coating on the walls of the nanotube. It should be noted that the DNA coating on the nanotubes was almost complete by day 35, coinciding with the time at which the absorbance spectra and PL spectra started to improve. Again, this suggests that the switch-on time for the absorption and PL spectra is linked to the completion of a DNA monolayer. It should also be noted that while the absorption spectra reached its maximum intensity by day 35, the PL intensity grew over a longer time scale, starting to increase on day 35 and reaching its maximum intensity by day 49, coinciding with the time at which a full monolayer coated the nanotubes according to calculations based on the CD data. Thus, it can be concluded that while the PL spectra are more sensitive to the degree of DNA coverage than the absorption spectra, changes in both the fluorescence and absorption properties are observed once a significant fraction of the nanotube walls are coated with DNA. Furthermore, the shift in the PL and absorption peak positions observed between days 28 and 35 is consistent with the removal of water from the interface between the nanotubes and their surroundings due to a change in the DNA coverage. The optical transition energies of SWNTs are influenced by the dielectric properties of their local surroundings,[51,52] and thus, the degree of wrapping and the level of interaction between the nanotubes and the surrounding water are all expected to cause changes in the absorption and PL peak positions.

According to molecular modeling studies, ss-DNA binds to a nanotube by wrapping helically around the nanotube.[30,43] Phase images from AFM have shown periodic helical wrapping of nanotubes by ss-DNA.[28,31] However, to our knowledge, no evidence for helical wrapping has been shown to date for

(69) Coleman, J. N.; Blau, W. J.; Dalton, A. B.; Munoz, E.; Collins, S.; Kim, B. G.; Razal, J.; Selvidge, M.; Vieiro, G.; Baughman, R. H. *Appl. Phys. Lett.* **2003**, *82*, 1682–1684.

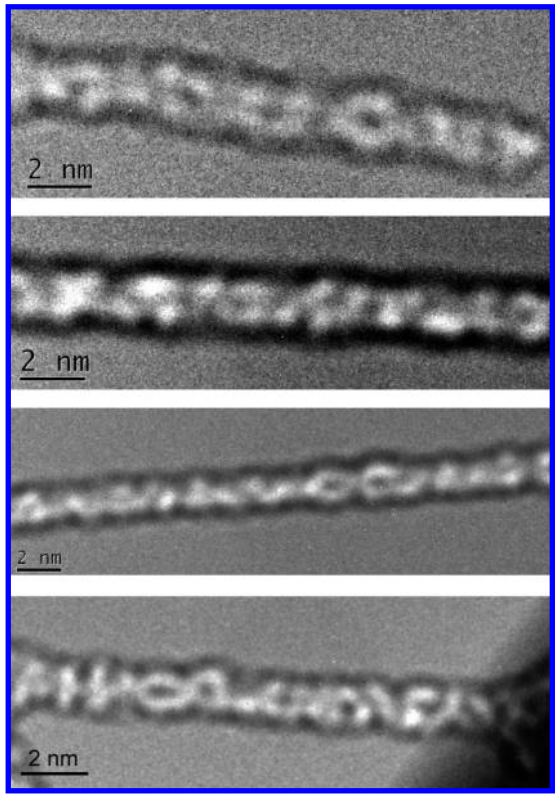

Figure 6. Various HRTEM images showing DNA wrapping of nanotubes in a 32 day old sample.

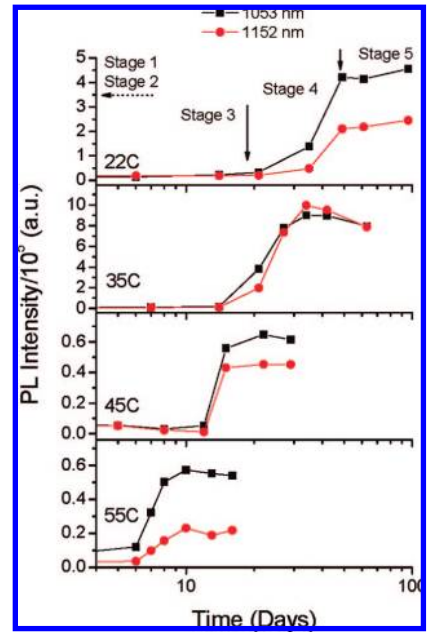

Figure 7. PL peak heights as a function of time for four different samples with temperatures ranging from 22 to 55 °C. The solid arrows approximately indicate τ_0 and τ_1. Also indicated are the time frames associated with the various stages 1 to 5 described in the text; the dotted arrow represents the fact that stages 1 and 2 occur very close to $t = 0$.

SWNTs dispersed with ds-DNA. In addition, DNA wrapping has never been observed using HRTEM for either ss- or ds-DNA. We therefore present the HRTEM images displayed in Figure 6, which show the helical wrapping of nanotubes by salmon testes DNA approximately 30 days after sample preparation. The majority of the images show the DNA appearing to crisscross itself along the length of the nanotube. In TEM, the electron beam is transmitted through the sample, making it impossible to differentiate between the front and back of the specimen. Thus, the DNA on both the front and back of the nanotube can be seen in these images. This implies that the majority of nanotubes are wrapped helically by two separate strands of DNA that are phase-shifted by 180° with respect to each other. This suggests that the mechanism of binding of ds-DNA to SWNTs is one in which the ds-DNA unzips onto the nanotube, allowing the two separated strands to interact with the nanotube. The phase shift of 180° between the two strands maximizes both the nanotube coverage and the distance between the negatively charged phosphates on the backbones of the strands. The individual strands all had pitches close to 2.2 nm. This is in agreement with the results of molecular dynamics simulations, which suggest that oligonucleotides such as $(GT)_{30}$ wrap around nanotubes with pitches between 2 and 8 nm.[49] In a minority of cases, the DNA appears to zigzag along the length of the nanotubes, suggesting that some of the nanotubes are wrapped by just one strand of DNA. In these cases, it is most likely that the DNA was already single-stranded when the wrapping began.

Temperature Studies. While the previous analysis shows clear evidence for the progressive wrapping of DNA around nanotubes and its influence on the solution's optical properties, it is still unclear what factors control this wrapping process and why the DNA coating should cause these changes. It was initially thought that the time taken for a DNA monolayer to form might be dependent on the rate at which the ds-DNA unzips into two separate strands. If this is correct, then increasing the sample temperature should increase the rate at which the DNA unzips and thus accelerate the formation of the DNA monolayer. Consequently, three similar samples were prepared at a nanotube concentration of 0.018 mg mL^{-1} and a DNA−SWNT ratio of 2:1 and maintained at temperatures of 35, 45, and 55 °C. As before, a time-dependent improvement in the absorption and NIR PL spectra coupled with a reduction in the CD intensity was observed. Figure 7 shows the PL peak heights as a function of time for each sample. In all cases, two characteristic times can be identified. The first characteristic time, τ_0, is the time that elapses before any increase in PL intensity is observed. This time decreased with increasing temperature and varied from 29 ± 7 days for the 22 °C sample to 6.5 ± 0.5 days for the 55 °C sample. The second characteristic time, τ_1, is the time at which the PL intensity reaches its maximum. This time also decreased with temperature and ranged from 42 ± 7 days in the 22 °C sample to just 9 ± 1 days in the 55 °C sample. These results suggest that the appearance of the PL is controlled by at least two processes, one characterized by a waiting time τ_0 and the other controlling the increase in PL with a characteristic rise time $\tau_1 - \tau_0$.

Interestingly, the emission peaks from large-diameter nanotubes that were missing in the 22 °C sample were present in the one at 35 °C. The magnitude of the spectrum was found to vary with temperature, with the most intense spectrum being observed for the 35 °C sample while the 45 and 55 °C samples were much less intense (Figure S5A in the Supporting Information). AFM analysis of the bundle diameters showed that the increase in PL intensity in the 35 °C sample cannot be attributed to debundling of nanotubes. The mean bundle diameter for the 35 °C sample was 2.5 nm, and the fraction of individual SWNTs was 0.74 for $d \leq 2.4$ nm or 0.35 for $d \leq 1.4$ nm. Thus, the change in the PL intensity must be due to a change in the

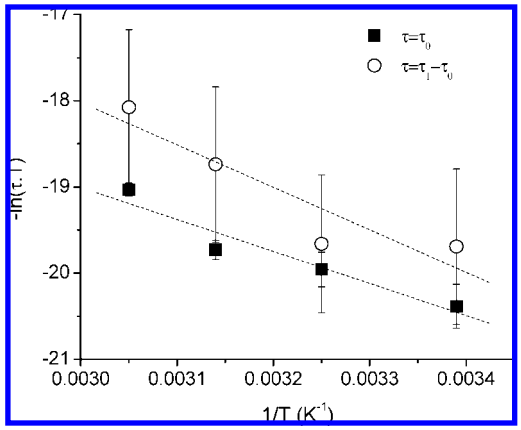

Figure 8. Eyring plots of the natural logarithm of the product of the experimental characteristic time and absolute temperature vs the inverse temperature. The characteristic times τ_0 and $\tau_1 - \tau_0$ relate to the time before PL appears and the time over which the PL increases, respectively. The activation energy of the rate-limiting step associated with each process can be calculated from the slope of the corresponding curve; values of 31 ± 6 and 41 ± 12 kJ mol^{-1}, respectively, were obtained. The associated activation entropies were found from the intercepts to be -263 ± 20 and -225 ± 40 J mol^{-1} K^{-1}, respectively.

interaction between the SWNTs and their surroundings. Visible aggregation was observed in both the 45 and 55 °C samples over time, which would account for the weak PL emission from these samples. For completeness, a similar 1 day old DNA−SWNT solution was refluxed at 110 °C for 1−4 h. Weak NIR PL emission and a slight improvement in the absorption spectra were observed after refluxing for 4 h (Figure S5B in the Supporting Information).

In order to gain a better understanding of the temperature dependence of the appearance of PL, the data was analyzed within the framework of activated complex theory using a modified version of the Eyring equation:

$$\frac{1}{\tau} = \frac{k_B T}{h} e^{-\Delta H^{\ddagger}/RT} e^{\Delta S^{\ddagger}/R} \quad (3)$$

where τ is the characteristic time, k_B is Boltzmann's constant, T is the absolute temperature of the system, h is Planck's constant, $\Delta H^{\ddagger}$ is the enthalpy of activation, R is the gas constant, and $\Delta S^{\ddagger}$ is the entropy of activation. We can think of the reciprocal of τ as a proxy for the rate of the process under investigation. Here we analyzed the data in terms of the waiting time τ_0 and the rise time $\tau_1 - \tau_0$ (see Figure 8). This allowed us to calculate $\Delta H^{\ddagger}$ and $\Delta S^{\ddagger}$ values relating to the rate-limiting steps associated with the processes occurring before PL turn-on (characterized by τ_0) and during the PL increase (characterized by $\tau_1 - \tau_0$). The $\Delta S^{\ddagger}$ values for these processes were calculated from the data in Figure 8 to be -263 ± 20 and -225 ± 40 J mol^{-1} K^{-1}, respectively. The activation entropy is negative in both cases, suggesting that the system is changing from a less-ordered to a more-ordered state. The $\Delta H^{\ddagger}$ values were calculated to be 31 ± 6 and 41 ± 12 kJ mol^{-1} (0.32 ± 0.06 and 0.43 ± 0.13 eV), respectively.

Thus, we can differentiate two separate rate-limiting processes that control the time taken for the quenching mechanism to dissipate. It is very important to explain these processes in relation to the physical mechanism of DNA wrapping of the nanotubes. First we need to consider the root cause of the quenching as opposed to the return of PL.

Mechanism of PL Switch-On: Role of O_2 and pH in PL Quenching. While we now know that the PL emission and van Hove absorption intensity increase dramatically upon the completion of a full monolayer of DNA coverage, little is yet understood about the processes controlling this sudden change. Computational studies have shown that these changes cannot be attributed to a change in the electronic structure of the nanotube as a result of interactions between the nanotube and DNA.[70] Intuitively, it would seem that the DNA coating must segregate the SWNT from its surroundings, shielding the nanotube from the surrounding water. As interaction with water is reported to decrease NIR PL emission through nonradiative decay processes, such shielding should result in increased PL intensity.[71] However, it is unlikely that this fully explains the results. Similar luminescence quenching has been observed for SWNTs dispersed with surfactants in water[61,72,73] when exposed to oxygen under low pH conditions. We suggest that the model proposed by Dukovic et al.[72] could help explain our results. In this mechanism, oxygen covalently bonds across a C_6 hexagon on the nanotube sidewalls, creating a 1,4-endoperoxide. The endoperoxide ring has no effect on the optical properties of the nanotube except under acidic conditions, where the endoperoxide ring opens and becomes protonated, leading to hole localization and a large decrease in the absorption and luminescence intensities as a result of Auger recombination. This effect is greatest for large-diameter nanotubes. Their study found that just 1 protonated endoperoxide per 40 nm of nanotube length was sufficient to completely quench the luminescence from the nanotube.[72] The SWNTs used throughout our experiments were handled in air. In addition, no effort was made to deoxygenate the water during sonication. Therefore, it is probable that the nanotubes had many surface oxides available for protonation. In addition, there should be sufficient numbers of protons in the water to protonate the endoperoxides and quench the NIR PL.

We suggest that the restoration of NIR PL in older samples is facilitated by the partial removal of protonated surface oxides from the nanotube walls plus the deprotonation of any remaining protonated endoperoxides. We propose that oxides are displaced from the nanotube by competitively binding to the DNA as it progressively covers the nanotube. The most probable mechanism for this is one in which the endoperoxides react with the nucleotide bases on the DNA.[74] Thus, NIR PL is restored some time after the DNA wrapping is complete and a significant fraction of surface oxides have either been deprotonated or removed and trapped by the DNA. This process would be enhanced in solutions stored at higher temperatures,[73] which may explain why the PL intensities are greater and the large-diameter emission peaks are present in the 35 °C sample.

In order to investigate this process further, three DNA−SWNT samples were prepared at a concentration of 0.02 mg mL^{-1} with a 10 mM phosphate buffer at pH 7, 8, and 8.8. Unlike the pH 7 sample, the two basic samples displayed PL emission peaks

(70) Wall, A.; Ferreira, M. S. *J. Phys.: Condens. Matter* **2007**, *19*, 406227.
(71) Strano, M. S.; Moore, V. C.; Miller, M. K.; Allen, M. J.; Haroz, E. H.; Kittrell, C.; Hauge, R. H.; Smalley, R. E. *J. Nanosci. Nanotechnol.* **2003**, *3*, 81–86.
(72) Dukovic, G.; White, B. E.; Zhou, Z.; Wang, F.; Jockusch, S.; Steigerwald, M. L.; Heinz, T. F.; Friesner, R. A.; Turro, N. J.; Brus, L. E. *J. Am. Chem. Soc.* **2004**, *126*, 15269–15276.
(73) Nish, A.; Nicholas, R. J. *Phys. Chem. Chem. Phys.* **2006**, *8*, 3547–3551.
(74) Ravanat, J.-L.; Di Mascio, P.; Martinez, G. R.; Medeiros, M. H. G.; Cadet, J. *J. Biol. Chem.* **2001**, *276*, 6056.

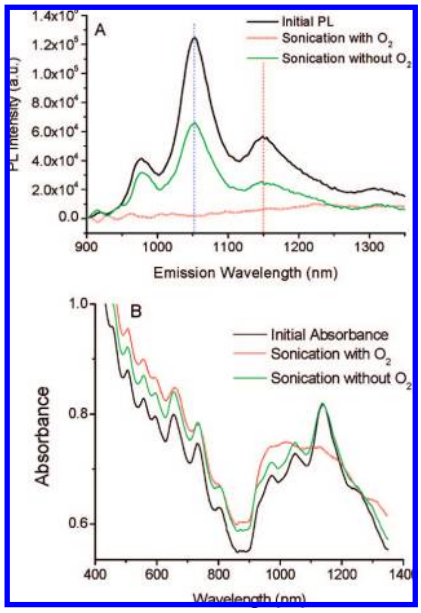

Figure 9. (A) NIR PL line spectra and (B) absorption spectra for the original, unaltered sample and for oxygenated and deoxygenated samples after sonication. Sonication in the presence of oxygen was found to quench photoluminescence and bleach the absorption spectrum.

immediately after preparation (the neutral sample exhibited no detectable photoluminescence at that time). The emission from the pH 8.8 sample was ~2.5 times stronger than that from the pH 8 sample. It was found that the NIR PL from the pH 7 and pH 8 samples grew steadily over the following two weeks, until the PL intensity was almost equal to that of the pH 8.8 sample (Figure S6 in the Supporting Information). Thus, although the PL emission is restored by increasing the pH of the sample, the same increase in PL is observed over time. Interestingly, it was found that the NIR PL intensities grew much faster in the pH 7 sample than in other samples that were dispersed in water without any buffer. It is possible that this was facilitated by interactions between the buffer and the phosphate groups in the DNA backbone.

Further investigation into the effect of oxygen on the optical properties of the system was carried out on an older sample. A 6 month old solution with well-defined absorption and PL spectra was split in two. N_2 gas was bubbled through one half of the sample for 5 min to remove dissolved oxygen while the other half of the sample was left unmodified. Both samples were then sonicated for 5 min in the sonic bath to partially remove the DNA coating (see below). The NIR PL spectra taken before and after sonication are shown in Figure 9A. It was found that the deoxygenated sample had partially retained its NIR PL emission, while the photoluminescence was completely quenched in the oxygen-rich sample. A similar effect was observed for the absorption spectrum of the samples. The deoxygenated sample retained its original absorption spectrum, while the oxygenated sample became bleached after sonication (Figure 9B). Both samples were stored under nitrogen and then analyzed over the following month. It was found that both samples regained their original PL intensities over time. However, the oxygenated sample took 35 days before NIR PL emission was observed again. This is similar to the time taken for the NIR PL to switch on after initial sample preparation.

Such quenching effects always occurred when the sample was sonicated without first removing the oxygen from the sample. This suggests that the sonication process plays an important role in the interaction of oxygen with the nanotube. The effects of sonication on the DNA−SWNT hybrid were investigated by AFM. A similar 6 month old sample was sonicated for 5 min, causing the PL emission to switch off. AFM images were recorded before and after sonication and used to calculate diameter distributions (Figure S7 in the Supporting Information). These were found to be statistically different, with a mean diameter of 2.1 nm before sonication and 1.5 nm after sonication. PL spectra recorded before sonication showed strong emission from the (8,3), (7,5), and (7,6) nanotube species, confirming that large quantities of these nanotubes were individually dispersed in the sample at this time. These nanotubes all have diameters smaller than 1 nm (0.77, 0.82, and 0.88 nm, respectively). However, in the unsonicated sample, less than 1% of the nanotubes measured by AFM had diameters smaller than 1 nm. Thus, as expected, the diameters measured before sonication show that the nanotube walls must be coated with DNA. After sonication, 38% of the measured nanotubes had diameters of less than 1 nm as a result of the removal of DNA from the nanotubes. The diameter distributions before and after sonication were found to be statistically indistinguishable to a significance level of 0.004 when an extra 1 nm was added to the diameters of the bundle after sonication to account for the DNA that had been removed. Thus, it was concluded that sonication removes DNA from the nanotube sidewalls. This discovery provides great insight into the previous experiment. When the deoxygenated solution was sonicated, the sample retained much of its PL spectrum despite the removal of the DNA from the nanotubes and the consequent exposure of the sidewalls. This suggests that there were very few surface oxides on the nanotube sidewalls available to interact with the protons in the water. By this logic, it must be assumed that there were very few endoperoxides on the DNA-wrapped nanotubes before sonication. This leads to the conclusion that the DNA wrapping facilitates the restoration of NIR PL emission by removing the majority of the surface oxides from the nanotubes and deprotonating the few remaining protonated endoperoxides.

It should be noted that in all of the samples at all times, the S_{11} absorption peaks were less intense than the S_{22} peaks, even when the PL emission intensities had fully saturated. It has been shown that for samples prepared with raw (not acid-purified) SWNTs, the S_{11} transitions are significantly more intense than the S_{22} transitions.[75] However, when purified SWNTs are used (as in this experiment), the intensity of the S_{11} transitions is considerably reduced. This phenomenon has been attributed to hole-doping due to residual $C{:}H^+$ moieties associated with the purification process.[75,76] This suggests that while DNA wrapping both removes and deprotonates protonated endoperoxides, it does not remove the functional groups created during the purification process. Thus, DNA wrapping restores the PL spectra to a typical spectrum for purified HiPCO SWNTs.

Mechanism of Wrapping. We are now in a position to consider the wrapping mechanism. The results described above can be distilled down to three pieces of information: (A) AFM studies showed that the nanotubes were stabilized against aggregation virtually immediately after sample preparation; (B) the CD results showed that the rate of denaturing of DNA was almost constant until one monolayer had formed; and (C)

(75) Blackburn, J. L.; McDonald, T. J.; Metzger, W. K.; Engtrakul, C.; Rumbles, G.; Heben, M. J. *Nano Lett.* **2008**, *8*, 1047–1054.
(76) Ramesh, S.; Ericson, L. M.; Davis, V. A.; Saini, R. K.; Kittrell, C.; Pasquali, M.; Billups, W. E.; Adams, W. W.; Hauge, R. H.; Smalley, R. E. *J. Phys. Chem. B* **2004**, *108*, 8794–8798.

analysis of the temperature-dependent PL results showed that the waiting time τ_0 and PL rise time $\tau_1 - \tau_0$ are controlled by distinct processes, both of which involve ordering.

Previously, it has been proposed that polymer wrapping of nanotubes in aqueous media is driven by the need to eliminate the hydrophobic interface between the nanotubes and the water. For example, in the case of poly(vinylpyrrolidone) interacting with an individual SWNT, the polymer−nanotube binding energy more than compensates for the entropic decrease on wrapping.[77] However, we note that the situation is somewhat more complicated in the case of ds-DNA, which already exists in a structured form before interacting with the nanotubes. Energy is required to denature the ds-DNA, a process that is also accompanied by a significant entropy increase. For example, the enthalpy associated with disruption of nearest-neighbor interactions within an existing duplex ranges from 23.4 to 49.8 kJ mol^{-1} while the entropy ranges from 56.4 to 116 J mol^{-1} K^{-1} for GA/CT and CG/GC, respectively, in 1 M NaCl.[78] However, while wrapping of ss-DNA around the nanotube is exothermic, a large entropic cost is associated with this process. In addition, the low $\Delta H^{\ddagger}$ values obtained for the DNA−SWNT samples imply that the mechanism of DNA wrapping cannot be one in which the DNA duplex fully dissociates before covering the nanotube walls. Rather, any denaturing process must involve the dissociation of a small number of base pairs, allowing spontaneous unzipping of the ds-DNA onto the walls of the nanotube. The dissociation of a small number of base pairs would only require activation energies on the order of a few tens of kilojoules per mole.[65]

This allows us to suggest a multistage wrapping mechanism. Initially, two processes happen simultaneously. Sonication begins to initiate partial nanotube exfoliation, as described by Strano et al.[71] In addition, the initial enthalpic barrier to DNA strand separation is overcome as base pairs at the strand ends dissociate to form frayed, dangling ends on the ds-DNA. This facilitates nucleation events whereby these dangling single-stranded ends associate with partially exfoliated sections of nanotube. The partial adsorption of this ds-DNA would be expected to sterically stabilize the nanotube. That the nanotubes were stabilized virtually immediately means that a partial coating forms at very early times (during sonication). It is very possible that the early DNA coating consists predominately of very short strands which are more mobile. This is supported by the observation of small objects bound to the nanotubes by TEM on day 1 (Figure 5). This fraying and adsorption process can be considered as stage 1. This and subsequent processes are illustrated in Scheme 1.

Stage 2 involves spontaneous unzipping of partially bound strands of ds-DNA. This unzipping is accompanied by the formation of disordered coatings over parts of the nanotube. The presence of such a disordered intermediate state has been suggested in molecular dynamics simulations of DNA wrapping.[49] This unzipping/coating process is accompanied by a drop in CD intensity. The continuous decay of the CD intensity tells us that adsorption and unzipping occurs continually over a time frame of ~50 days (at room temperature) until the first monolayer is formed. The unzipping/coating procedure is driven partly by the reduction in energy due to the binding of DNA to the nanotube surface and partly by the gain in entropy due to unzipping and the formation of a disordered coating. An analogous system in nature involves the separation of ds-DNA helices into ss-DNA during the transcription process. Two competing models exist to describe this process.[79] The first is the "passive" unwinding mechanism, in which the DNA junction is opened transiently as a result of thermal fluctuations, providing enzymes (helicases) access to bubbles in the structure that allows them to move the junction forward, thereby catalyzing the unwinding of the ds-DNA. Thus, the helicase unwinds the DNA by trapping thermally frayed single strands of DNA. The second mechanism involves "active" unwinding, in which the helicase actively destabilizes the ds-DNA at a junction. Thus, in the DNA−SWNT system, the nanotube can be considered to contribute to activating the unwinding of ds-DNA.

Scheme 1. Various Stages of the Wrapping of DNA around Nanotubes (the Five Stages Are Described in the Text; Stage 5 Is Not Shown but Consists of the Formation of Successive Layers after the Monolayer)

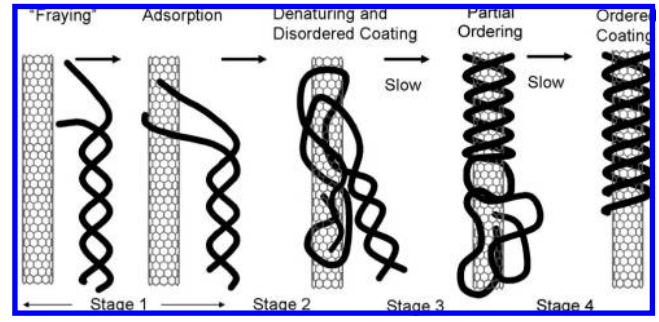

The next stage (stage 3) involves progression from a disordered wrapping state to one where sections of DNA strands form ordered, helically wrapped domains. We envisage that each DNA strand may contribute to both ordered and disordered regions, as illustrated in Scheme 1. As time moves on, the fraction of each DNA strand contributing to ordered domains increases at the expense of the fraction contributing to disordered domains. This process is characterized by the new orientation of the bases, which lie flat on the surface of the nanotube, thus increasing the binding energy. Again, this process has an entropic cost associated with the relative ordering and thus is very slow. The ordered domains are characterized by close contact between the bases and the nanotube. Under these circumstances, the probability that the surface oxides can transfer from the nanotube to the DNA is significantly enhanced. This results in the loss of exciton quenching sites from the nanotube surface. At some point, the first ordered domain reaches a critical length that is greater than the excursion range of an exciton. All of the associated protonated endoperoxides either transfer from the nanotube to the DNA or deprotonate, creating a long pristine section of nanotube. This is a significant event. Any excitons formed in this region will not encounter quenching sites and so may decay radiatively. Only then is the first PL observed. The critical length must be similar to the range of an exciton in an SWNT, which has been estimated to be ~90 nm.[80] Thus, because the time taken for fraying, adsorption, unzipping, and disordered coating to occur is expected to be relatively short,

(77) O'Connell, M. J.; Boul, P.; Ericson, L. M.; Huffman, C.; Yuhuang, W.; Haroz, E.; Kuper, C.; Tour, J.; Ausman, K. D.; Smalley, R. E. *Chem. Phys. Lett.* **2001**, *342*, 265–271.
(78) Breslauer, K. J.; Frank, R.; Blocker, H.; Marky, L. A. *Proc. Natl. Acad. Sci. U.S.A.* **1986**, *83*, 3746–3750.
(79) Johnson, D. S.; Bai, L.; Smith, B. Y.; Patel, S. S.; Wang, M. D. *Cell* **2007**, *129*, 1299–1309.
(80) Cognet, L.; Tsyboulski, D. A.; Rocha, J. D. R.; Doyle, C. D.; Tour, J. M.; Weisman, R. B. *Science* **2007**, *316*, 1465–1468.

the waiting time τ_0 is determined by the time for significantly large ordered sections (and the associated oxide transfer) to occur.

After this time, the PL intensity increases steadily. This is due to two occurrences. First, more and more 90 nm sections of ordered DNA appear. Second, existing 90 nm sections evolve into longer sections at the expense of the disordered sections (stage 4). When the DNA moves from a disordered coating to an ordered one, the strands become more compact, covering less of the nanotube's surface area. This has recently been demonstrated by molecular dynamics simulations.[49] This creates more exposed surface, allowing new ds-DNA strands to adsorb and start the whole process again. We expect this process to advance to an equilibrium in which the entire surface is coated with DNA. We also expect this coating to be dominated by ordered segments but possibly have a minority population of disordered segments. Thus, the rise time $\tau_1 - \tau_0$ is a measure of the time from the first appearance of a ~90 nm ordered section to the time when equilibrium develops.

After the formation of this ordered monolayer coating, DNA continues to adsorb onto the DNA-coated nanotube to give a multilayered structure. The onset of formation of the second monolayer is signaled by the decrease in the rate of denaturing shown in Figure 4C. Evidence for the formation of this multilayered structure is provided by HRTEM images, as shown in Figure 5D. This process can be considered as stage 5.

Conclusion

In conclusion, it was found that significant changes in the intensity and position of both the absorption and NIR PL van Hove peaks of DNA-dispersed SWNTs were observed over time. Bundle diameter distributions calculated from AFM images showed that these changes could not be correlated to a change in the number of individual SWNTs. CD was used to measure the concentration of free DNA in solution. This was found to decrease continuously over the duration of the experiment, suggesting that the fraction of DNA bound to the SWNTs increases with time. HRTEM images of the DNA-SWNT hybrids were obtained and clearly showed the progressive formation of a DNA coating over time. The changes in the SWNTs' optical properties were found to coincide with the time at which a full monolayer of DNA coated the SWNTs, as measured by HRTEM and CD. In addition, HRTEM images recorded at this time clearly showed helical wrapping of the DNA around the SWNTs.

The rate of DNA wrapping was investigated with respect to the sample temperature. It was found that the time required for a complete DNA monolayer to form on the SWNTs is controlled by a rate-limiting process with an activation enthalpy of 41 kJ mol^{-1} (0.43 eV). This low energy barrier is attributed to the final important step in the wrapping mechanism, which involves the transformation of the disordered population of DNA at the surface into a tightly bound array approximating a monolayer coating. We suggest that the underlying mechanism for the improvement of the optical properties is based on the removal or deprotonation of protonated surface oxides from the nanotube walls by the DNA. This effect can be further facilitated by heating the sample to 35 °C, yielding a 2-fold improvement in the NIR PL intensity and restoring the fluorescence from the wide-diameter SWNTs.

These experimental results lead to some interesting conclusions. First, as in the case of surfactant-based dispersions,[75] the sharpness and intensity of the absorption transitions in aqueous DNA−SWNT samples does not depend solely on the level of bundling in the system; the absence of a PL signal does not necessarily correspond to the absence of individually dispersed SWNTs in the sample. Second, the temperature dependence of the fluorescence spectrum means that using NIR PL to compare the populations of nanotube species in a sample is not a straightforward task.

Experimental Procedures

A nanotube dispersion was prepared at a nanotube concentration of 0.025 mg mL^{-1} by sonicating HiPCO SWNTs (www.cnano-tech.com, lot no. P0184) with double-stranded salmon testes DNA (purchased from Aldrich, product number D1626) at a DNA−SWNT mass ratio of 2:1 in D_2O, as described previously.[27] The DNA and SWNTs were sonicated together for 2 h in a round-bottom flask using a Branson 1510 sonic bath (with a frequency of 42 kHz and a rated power output of 80 W). The dispersions were sonicated in ice water, preventing the temperature from rising above 8 °C. Mild centrifugation (3300*g*) was employed in order to remove from the sample the very large aggregates that were not dispersed during sonication.[11] The nanotube concentration after centrifugation was ascertained using absorption spectroscopy and found to be 0.018 mg mL^{-1}, equating to a loss of 28%. The solution was kept in a darkened container at room temperature (~22 °C) and monitored weekly using five different methods of analysis over the subsequent 3 months. UV−vis−NIR absorption spectra were recorded using a PerkinElmer Lambda 900 spectrophotometer in order to probe the nanotubes and monitor the concentration of the sample. CD spectra were recorded using a Jasco J-810 spectropolarimeter in order to check for changes in the conformation of the DNA. NIR PL line spectra were recorded using an Edinburgh Instruments FLS920 fluorescence spectrometer with a Hamamatsu R5509 NIR photomultiplier tube in order to probe the individual semiconducting nanotubes. The samples were excited at a wavelength of 655 nm, and emission was detected over a wavelength range of 900−1400 nm. AFM analysis using a multimode Nanoscope III atomic force microscope in tapping mode was carried out in order to check for changes in the nanotube/bundle diameters. POINTPROBE silicon cantilevers with a typical tip diameter of ~80 nm were used throughout. The large size of the AFM tip in comparison with the diameter of a nanotube introduced significant tip effects in lateral measurement, making the nanotubes appear considerably larger than their actual size in the *xy* plane. Consequently, all of the diameters were established by measuring the nanotube heights (*z* direction). Finally, HRTEM images of the DNA−SWNT complexes were recorded regularly in order to check for changes in the degree of DNA coverage on the nanotube sidewalls over time. Small volumes of the sample were dropped onto holey carbon TEM grids and left to dry under ambient conditions before imaging with an FEI Technai F20 HRTEM instrument at an acceleration voltage of 200 kV and a JEOL 400F HRTEM instrument at an acceleration voltage of 100 kV.

Supporting Information Available: Figures S1−S7. This material is available free of charge via the Internet at http://pubs.acs.org.

JA803273S